ISSN 0965-545X, Polymer Science, Series A, 2020, Vol. 62, No. 3, pp. 260–271. © Pleiades Publishing, Ltd., 2020.
Russian Text © The Author(s), 2020, published in Vysokomolekulyarnye Soedineniya, Seriya A, 2020, Vol. 62, No. 3, pp. 207–219.

COMPOSITES

The Effect of Cold Rolling on the Mechanism of Fracture of an In Situ Filled Polypropylene–Graphene Plates Composite

A. V. Efimov[a], P. M. Nedorezova[b], S. L. Bazhenov[b,*], O. M. Palaznik[b], T. E. Grokhovskaya[a], and S. V. Polschikov[b]

[a] *Department of Chemistry, Moscow State University, Moscow, 119899 Russia*
[b] *Semenov Federal Research Center of Chemical Physics, Russian Academy of Sciences, Moscow, 119991 Russia*
**e-mail: sergey.l.bazhenov@gmail.com*

Received July 22, 2019; revised October 1, 2019; accepted October 15, 2019

Abstract—The influence of cold rolling on the mechanical characteristics of polypropylene saturated with particles consisting of three to five monolayers of graphene (the degree of filling of 0.2–3.5 wt %) is studied. The nanocomposites are obtained by in situ filling, i.e., synthesis of the polypropylene matrix on the particles, thus allowing more uniform distribution of the filler throughout the bulk of the matrices. The filling makes it possible to increase the Young modulus of the material. A certain fraction of particles assemble to form agglomerates, and another fraction of particles are uniformly distributed in the matrix. The agglomerates already lead to the embrittlement of unrolled polypropylene at a degree of filling of 0.2 wt %. Cold rolling suppresses the brittle behavior of the composite irrespective of the method of reduction of the particles of graphite oxide (chemical or thermal reduction). As a result of preliminary cold rolling, the elongation at break and strength of filled polypropylene sharply increase (depending on the degree of cold rolling and concentration of the filler, the elongation at break increases 50- to 100-fold, and the strength increases 1.5- to 2.0-fold). In the initial material, the agglomerates initiate the appearance of local fluidity microzones where rhombohedral microcracks fracturing the composite are conceived. No microzones appear at a degree of cold rolling $\Lambda = 1.25$, while no neck is observed either at $\Lambda = 1.9$. After cold rolling to a value of $\Lambda = 1.25$, pore formation upon further stretching disappears.

DOI: 10.1134/S0965545X20030062

INTRODUCTION

Increased interest has been aroused by the creation of polymer composite materials reinforced by a nanosized lamellar filler in recent years. The relatively low concentration of such a filler makes it possible to substantially increase the Young modulus, thermal conductivity, electric conductivity, and other characteristics of polymers.

Graphene-like particles are a promising reinforcing filler for polymer matrices owing to their lamellar shape, electrical conductivity, high strength, and a relatively low cost. A graphene-like filler is generally obtained by the reduction of graphite oxide, which in turn is obtained by the oxidation of a graphite powder by potassium permanganate in concentrated sulfuric acid in the presence of sodium nitrate (by the Hummers method) [1–4]. When placed in a preheated oven, graphite oxide explodes to form plates consisting of several (one to ten) monolayers [5, 6]. Sometimes, graphite oxide particles are chemically reduced.

Nanocomposites are synthesized by in situ filling, i.e., synthesis of the polypropylene matrix on graphene-like particles [7, 8], which makes it possible to more uniformly distribute the filler throughout the bulk of the matrix when compared to mechanical mixing in a melt. The main disadvantage of filled polymers is the brittleness under stretching and bending [9–12]. At low degrees of filling, composites based on plastic polymers behave as the unfilled matrix, but they generally become brittle in the case of an increase in the concentration of the filler.

This work does not consider composites based on brittle polymers, in which particles and short fibers increase the fracture toughness. The increase in the brittleness of filled thermoplastic matrices has two main causes, namely, the formation of a neck in the polymer under stretching and initiation of cracks by large particles [13–15]. If small microparticles are used, the formation of the neck can be named the main reason for the embrittlement of the composite. The strain in the neck depends on the type of polymer; its value is 300–800%. The fracture of the composite is determined by reaching the fracture strain in the neck, outside which the strain does not exceed 10–15%. [13]. The length of the zone of plastic deformation is short, and because of this, the macroscopic (mean) fracture strain is small despite the local plas-

ticity in the neck being formed. Such a behavior is called quasi-brittle. On the other hand, composites based on the polymers that become deformed without a neck are generally not embrittled [13]. They become uniformly elongated until the fracture strain is reached. This strain can be severalfold lower when compared to the initial polymer matrix, but the composite nevertheless remains plastic. For example, rubber and ultra-high-molecular-weight PE are not embrittled to the degree of filling of 60 vol % [16, 17]. In this case, the critical degree of filling upon the transition to the brittle behavior is determined by several factors, the most important of which is the strain strengthening of the matrix [18, 19].

The second reason for the brittle behavior of a composite consists in the presence of large particles that initiate the appearance of pores transforming to microcracks. The exfoliation of large particles and appearance of oval pores that are transformed to rhomboidal microcracks with the increase in the strain was observed in composite materials based on partially crystalline thermoplastics (HDPE, LDPE, PP) [13]. The transformation of an oval pore to a microcrack occurs upon reaching the critical opening of the pore, which is a characteristic of the material. The critical size of the particles near which a rhomboidal microcrack is formed is determined by the crack resistance of the matrix polymer and strain ratio λ [14, 15]:

$$D_c = \frac{G_{Ic}}{\sigma_{ym}(\lambda - 1)}, \quad (1)$$

where G_{Ic} is the fracture toughness of the polymer and σ_{ym} is the yield point of the polymer. The critical size of the particles decreases upon an increase in the strain ratio λ. If λ is lower than the strain ratio in the neck, the neck being formed undergoes fracture. The fracture is determined by reaching the critical elongation, at which the growth of defects starts. The influence of the filler on the fracture toughness of filled composites was studied by the authors of [20–23].

Orientation suppressing the formation of a neck can be called an effective method of increasing the plasticity of polymers [24, 25]. Cold rolling of a polymer film between two rollers is one of the orientation methods [26–34]. It turned out to be possible to suppress the brittle fracture of polyethylene filled with rubber particles by cold rolling [20]. Biaxial orientation made it possible to suppress the brittle fracture of PP and poly(butylene succinate) filled with rigid nanoparticles [35, 36].

The influence of cold rolling on the behavior of the polymers reinforced by lamellar nanofillers was not studied earlier.

The aim of this work is to study the influence of cold rolling on the mechanical properties of PP filled with graphene-like nanoplates and mainly on the stress–strain characteristics and structure of the composites. It is important that the utilized PP was distinguished by increased rigidity and propensity to brittle fracture owing to the characteristic features of the polymer obtained over metallocene catalysts [37].

OBJECTS AND METHODS OF STUDY

Composites based on isotactic PP filled with graphene-like nanoplates synthesized by the thermal or chemical reduction of graphite oxide were studied. Graphite oxide was obtained according to the modified Hummers method via the oxidation of a graphite powder by potassium permanganate $KMnO_4$ in concentrated H_2SO_4. The thermal reduction of graphite oxide was performed in an argon flow in an oven preheated to 900°C, where the particles exploded to form many flat particles (TRG). In the case of chemical reduction, an aqueous suspension of graphite oxide was treated by ultrasound in the presence of hydrazine hydrate at 70°C and then in an argon flow at 900°C for 1 h (CRG). The C : O ratio was 42.6 and 44.9 after the thermal and chemical reduction of graphite oxide, respectively. The BET specific surface area was 620 and 510 m^2/g for thermally and chemically reduced graphene, respectively [3]. The numerals at the abbreviations TRG and CRG describe the weight fraction of the particles.

The X-ray phase analysis of the powders was conducted on an ADP-1 diffractometer. The interlaminar distance was determined by the Wulff–Bragg formula

$$d_{002} = \lambda/2\sin\theta.$$

Here, $\lambda = 0.154$ nm is the wavelength of CuK_α radiation and 2θ is the diffraction angle. The sizes of the crystallites along the c axis were found by the formula

$$L_c = 0.94\lambda/\beta_{002}\cos\theta,$$

where β_{002} is the angular half-width of the line in radians. A peak at a scattering angle $2\theta = 26.6°$ is observed in the X-ray diffraction pattern of natural graphite, which corresponds to an interlaminar distance d = 0.335 nm. In oxidized graphite, the peak shifts to a region of smaller angles (10.8°), which corresponds to d = 0.822 nm. The increase in the interlaminar distance occurs owing to the intercalation of water molecules and formation of oxygen-containing functional groups between the graphite layers [38, 39]. A wide peak is seen in the X-ray diffraction patterns at 19.1° (d = 0.473 nm) and 18.8° (d = 0.466 nm) for chemically and thermally reduced particles, respectively. The disappearance of the peak of graphite oxide and the appearance of wide peaks in the region of large angles indicate the production of graphene-like materials. The values of L_c = 1.127 and 1.003 nm were cal-

culated for the chemically and thermally reduced particles, respectively. This corresponds to three to five monolayers at the interlaminar distance of graphite plates of 0.335 nm.

The synthesis of PP and composite materials was carried out on graphene-like particles in the bulk of liquid propylene in the presence of a catalyst system based on *ansa*-zirconocene *rac*-$Me_2Si(2\text{-}Me\text{-}4PhInd)_2ZrCl_2$ activated by methylaluminoxane [40, 41]. The filler particles were preliminarily treated in a medium of toluene, followed by ultrasound treatment in the presence of methylaluminoxane for 20 min. The polymerization was conducted at 60°C and a pressure of about 2.5 MPa in a reactor with a stirrer. The obtained PP was isotactic and had a high degree of crystallinity of ~62% and $M = 600–700 \times 10^3$. The degree of filling was controlled by changing the amount of the filler, time of polymerization, and concentration of the catalyst [40, 41].

Films with a thickness of 300 μm were pressed at 190°C and a pressure of 10 MPa, after which they were cooled at a rate of 15 K/min (films with a thickness of 100–200 μm were used in individual experiments). The films were rolled on laboratory rollers at room temperature between two rollers rotating at the same speed. As a result of cold rolling, the length of the samples increased, the thickness decreased, and the width remained unchanged. The degree of cold rolling Λ was estimated as the ratio of the initial thickness d_0 to the thickness of the rolled film d: $\Lambda = d_0/d$. The value of Λ was varied from 1.1 to 2.0 by changing the width of the gap between the rollers.

Samples in the form of a two-sided blade with the width and length of the working part of 6 × 20 mm, respectively, were cut out from the films along the direction of cold rolling. The samples had the dimensions of 4 × 6 mm in some experiments. The stretching was performed under ambient conditions on an Instron 430 universal testing machine at a speed of 5 mm/min.

The composite materials were studied on a JSM-5300LV (Jeol) scanning electron microscope (SEM) and a LEO-912AB transmission electron microscope. The low-temperature chippings of the samples cooled in liquid nitrogen and split along their axis were observed under the scanning electron microscope. Ultrathin sections with a thickness of 50 nm for the transmission electron microscope were prepared on a microtome.

The thermophysical properties of the materials were determined by DSC on a TA-4000 thermal analyzer (Mettler) with a DSC-30 low-temperature cell. The rate of heating was 10 K/min. Samples with a weight of 0.5–2.0 mg were used. The degree of crystallinity of polypropylene was calculated by the formula

$$\chi = \frac{\Delta H}{\Delta H_{100\%}} \times 100\%.$$

Here, ΔH is the experimentally obtained heat of melting of PP and $\Delta H_{100\%} = 165$ J/g is the heat of melting of an ideal crystal of PP [25].

The structure of isotactic PP and composites based on it were studied by small-angle X-ray scattering on the DIKSI unit at the Kurchatov Complex for Synchrotron and Neutron Investigations. The wavelength of X-ray radiation was 0.162 nm. The distance between the sample and a Dectris Pilatus3R 1M detector was 2.4 m, and the time of exposition of the samples was 180–300 s. Silver behenate was used as the reference sample. The size of a pixel in the scattering pattern was 172 μm. To obtain the distribution of the intensity of scattering of X-rays depending on the value of the scattering vector, the Fit 2d program was used. The amplitude of the scattering vector q was calculated as

$$q = 4\pi\sin\theta/\lambda,$$

where 2θ is the scattering angle and $\lambda = 0.162$ nm is the wavelength of X-ray radiation. The distributions were normalized to the intensity of the primary beam, absorption, exposition, and thickness of the sample. The value of the long period was found from the scattering curves: $L = 2\pi/q_{max}$ (q_{max} corresponds to the maximum of the curve).

The radius of gyration of the graphene-like particles in the composites was calculated on the basis of the Guinier formula [42]

$$\ln I = \text{const} - q^2 R_g^2/3.$$

Here, I is the intensity of scattering and R_g is the radius of gyration of the particles. R_g of the particles was determined by the initial inclination of the curves of small-angle scattering in $\ln I–q^2$ coordinates.

RESULTS AND DISCUSSION

Microstructure of the Composites. Mainly, the structure of the composites filled with thermally reduced graphene was studied in this work. Figure 1 shows a thin section of a rolled PP–3.3% TRG composite under a transmission electron microscope. The filler is nonuniformly distributed in the polymer, and zones with an excess of the matrix are seen. The plates of the filler are bent, and their typical length is ~100 nm. The oblong shape of the plates provides the reinforcement of the polymer. No pores are observed, and the particles are predominantly vertically orientated in the direction of the axis of cold rolling.

Small-Angle X-Ray Patterns

Figure 2 presents the distributions of the intensity of small-angle X-ray scattering by polypropylene (curve *1*) and unrolled composites based on it (curves *2*, *3*). The curves are normalized to the absorption and thickness of the sample. A maximum at $q = 0.49$ nm^{-1} is seen in small angles in unfilled PP.

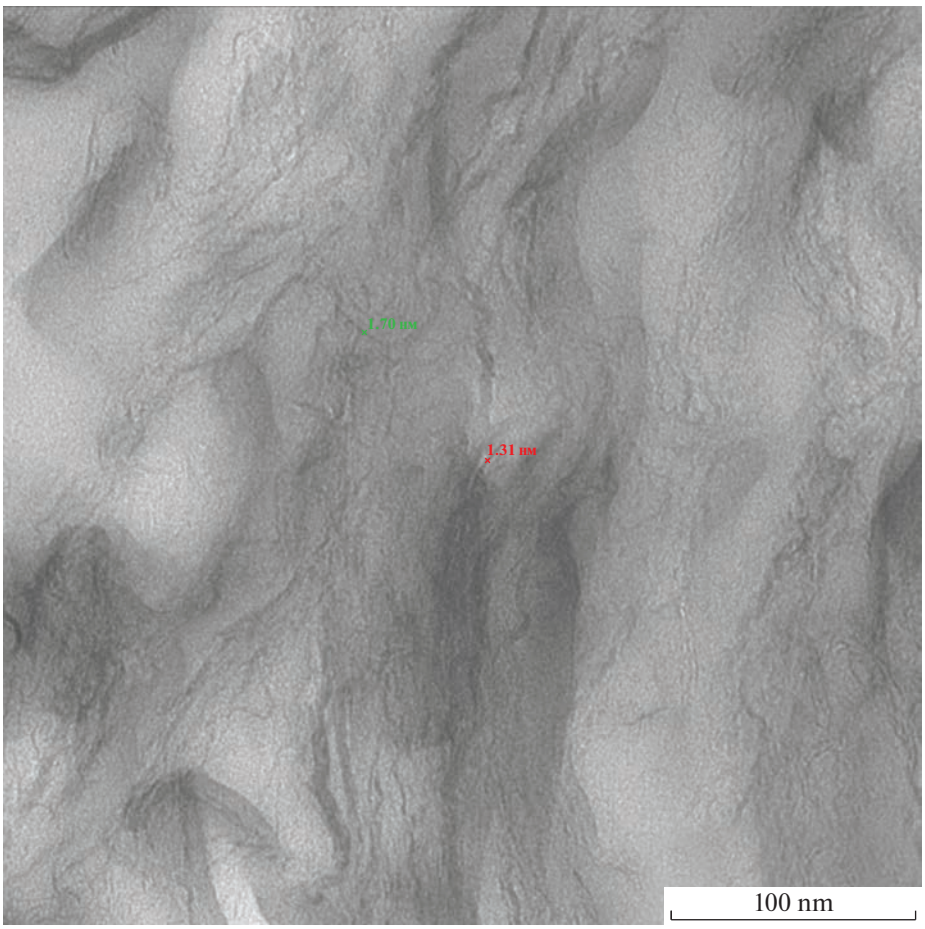

Fig. 1. Microtome section of a rolled PP–3.3% TRG composite under a transmission electron microscope; the degree of cold rolling $\Lambda = 2.K$

The long period is calculated by the formula $L = 2\pi/q_{max}$ and is 13 nm, which is interpreted as the distance between the centers of the lamellae. The composites scatter X-rays in the region of small angles by about an order of magnitude more intensely when compared to unfilled PP. This is determined by the significant difference in the density of graphene and polypropylene. The value of the radius of gyration of the particles of graphene determined from the curves of small-angle scattering is 38 nm.

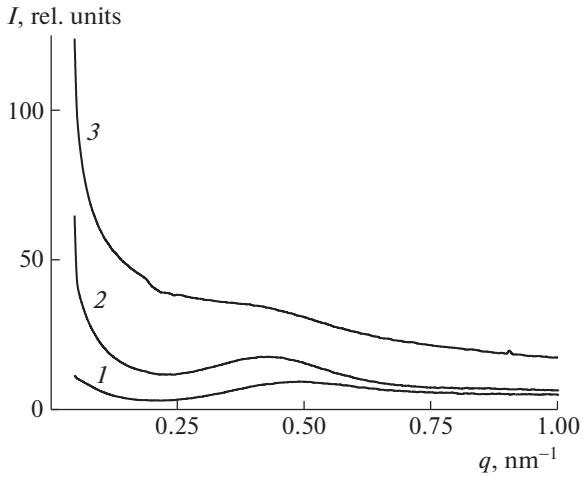

Fig. 2. Dependence of the intensity of small-angle X-ray scattering on the amplitude of the scattering vector q for (*1*) unrolled PP and (*2*, *3*) composites based on it with the concentration of the particles of TRG of (*2*) 0.2 and (*3*) 3.3 wt %.

Thermophysical Properties of Unfilled PP

Isotactic PP obtained over metallocene catalysts is a partially crystalline polymer in a monoclinic α-form. Table 1 presents the thermophysical characteristics of the initial and rolled filler-free PP. Cold rolling does not change the glass transition temperature or the degree of crystallinity of the polymer. The degree of crystallinity of the polymer is ~62%. The glass transition temperature of PP is 5°C. According to the data obtained earlier by atomic force microscopy, PP has a spherulitic structure with the size of the spherulites of 3–5 μm.

Table 1. Influence of cold rolling on the temperature and heat of melting of unfilled PP (the rate of heating is 10 K/min)

Degree of cold rolling of PP	Melting point, °C	Heat of fusion, J/g	Degree of crystallinity, %
Unrolled	157	102	62
1.25	157	99	60
1.50	158	104	63
1.90	157	104	63

Mechanical Properties of Unfilled PP

The stress–strain curves of unfilled PP with different degrees of cold rolling Λ are shown in Fig. 3. The unrolled polymer (curve *1*) undergoes deformation with the formation of a neck, and a characteristic yield drop is observed on the diagram. The formation of the neck started from the appearance of a shear band at the yield stress. The polymer in the shear band and neck became turbid as a result of formation of micropores.

Unoriented PP underwent fracture soon after the propagation of the neck along the entire working part of the sample, and the fracture strain was close to the strain in the neck. It is known that polymers with unexpressed strain strengthening are embrittled at very low degrees of filling [11, 12].

A neck was also formed in the samples at low degrees of cold rolling (Λ = 1.25–1.50), but the transition to it was diffused rather than sharp as in the initial PP. The strain ratio in the neck and difference between the upper and lower yield points (the height of the yield drop) decreased as a result of cold rolling. At the degrees of cold rolling Λ = 1.2–1.5, the main elongation was no longer in the neck but at the stage of strain strengthening. No neck appeared at Λ = 1.9, and the stress monotonically increased with the strain. The rolled samples remained transparent up to the strain of 500–700%, which indicates the absence of micropores. Here, the inclination of the final section of the stress–strain curves increased, i.e., the strain strengthening of the polymer intensified as a result of its molecular orientation.

The dependence of the strain ratio in the neck λ_n on the degree of cold rolling Λ is presented in Fig. 4. It is seen that λ_n sharply decreases with the growth in Λ. For example, $\lambda_n = 6.5$ for the initial polymer, while it decreases to ~3 already at Λ = 1.25.

Figure 5 shows the dependence of the ultimate stress and upper and lower yield points of unfilled PP on the degree of cold rolling Λ. The tensile stress at break is proportional to Λ as in other polymers [24, 25, 43]. On the other hand, the yield point first decreases from ~36 MPa for the unrolled polymer to ~32 MPa at Λ = 1.25, but then increases. The decrease in the

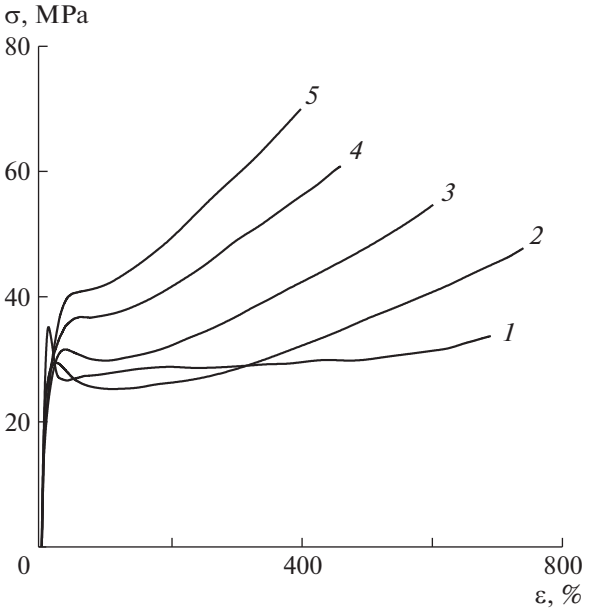

Fig. 3. Stress–strain curves of the (*1*) initial PP and (*2–5*) PP rolled at Λ = (*2*) 1.25, (*3*) 1.5, (*4*) 1.7, and (*5*) 1.9.

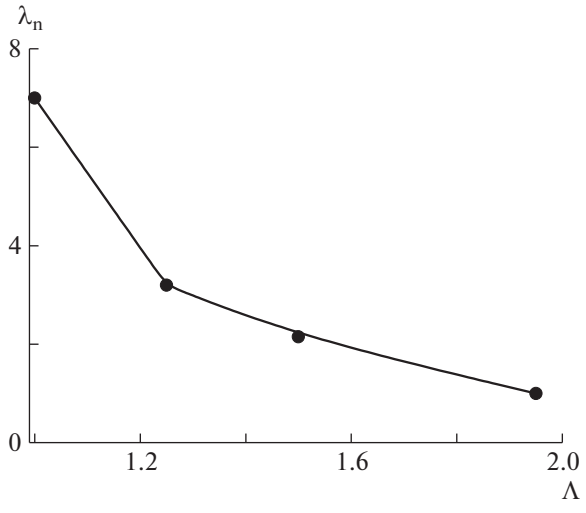

Fig. 4. Dependence of the strain ratio in the neck λ_n of unfilled PP on the degree of cold rolling Λ.

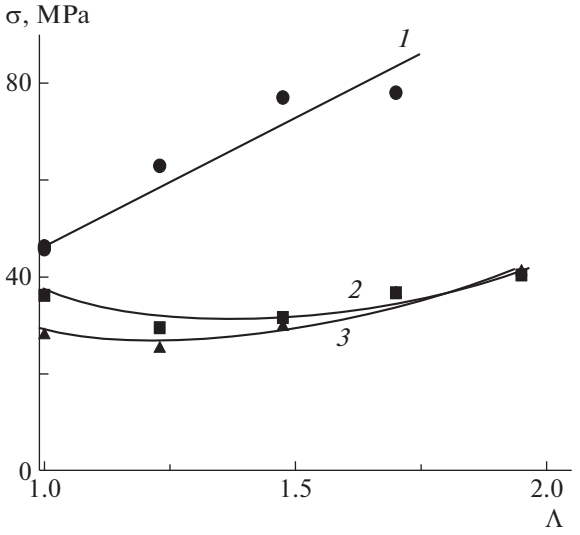

Fig. 5. Dependence of the (*1*) ultimate stress and (*2*) upper and (*3*) lower yield points of PP on the degree of cold rolling Λ.

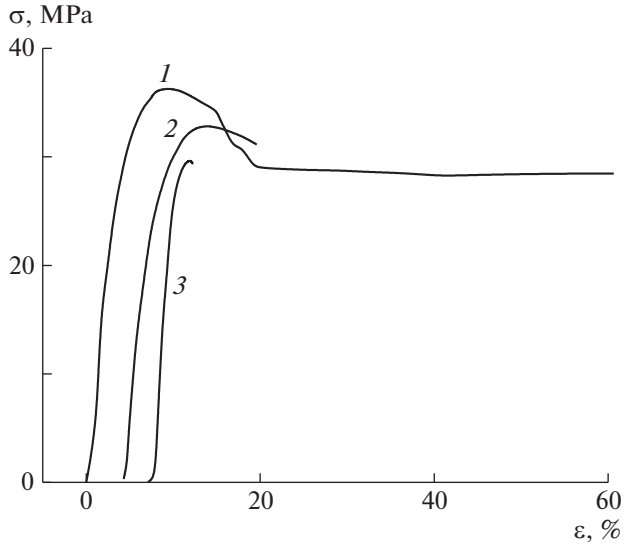

Fig. 6. Initial sections of the stress–strain curves of (*1*) unrolled PP and (*2*, *3*) composites containing (*2*) 0.2 and (*3*) 3.3 wt % TRG (the elongation at break of unrolled PP is 700%).

yield point after deformation is called true strain softening. This effect is less pronounced in amorphous/crystalline polymers than in glasslike polymers, but it is also noticeable in PP. A small minimum at $\Lambda = 1.25$ is also traced in the dependence of the lower yield point (curve *3*).

Mechanical Properties of the Unrolled Composite

The influence of the particles on the stress–strain curves is illustrated by Fig. 6. Unfilled PP is plastic, but already at the filling $V = 0.2$ wt % with thermally reduced particles of graphene, the material underwent fracture during the process of formation of the neck, and its fracture strain decreased ~40-fold in comparison with unfilled PP. The composite underwent fracture without reaching the yield point at the concentration of the particles $V = 3.3$ wt %. The respective fractured sample is shown in Fig. 7. The fracture was brittle, without traces of plastic deformation.

Therefore, the initially plastic PP already became quasi-brittle at a degree of filling of 0.2 wt % and brittle at 3.3 wt %. The composite behaved in a similar manner in the case of chemically reduced particles, but the embrittlement occurred at somewhat higher values of the concentration of the filler. For example, it fractured during the formation of the neck at the concentration of the particles of 1.8 wt %.

The influence of the filler on the Young modulus E of the material is demonstrated by Fig. 8. The introduction of the particles leads to an increase in the Young modulus, but a substantial growth is observed at the degrees of filling of at least 2–3 wt %. Note that the Young modulus of the studied PP is higher when compared to the industrial brands; this is associated with the increased degree of crystallinity owing to the catalyst used.

Structure and Mechanical Properties of the Rolled Composites

The small-angle X-ray diffraction patterns of the rolled PP–3.3% TRG composites are presented in Fig. 9. The particles lead to a sharp increase in scattering (Fig. 9b). Cold rolling changes the character of scattering. The reflection becomes elongated along

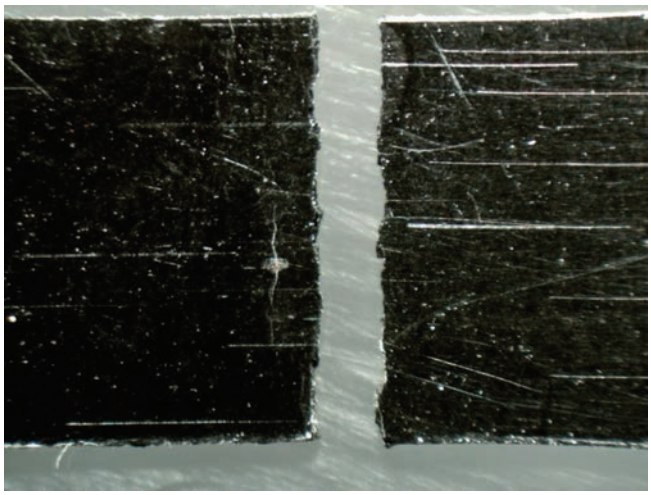

Fig. 7. Optical photographic image of the unrolled sample of PP–3.3% TRG; ×15.

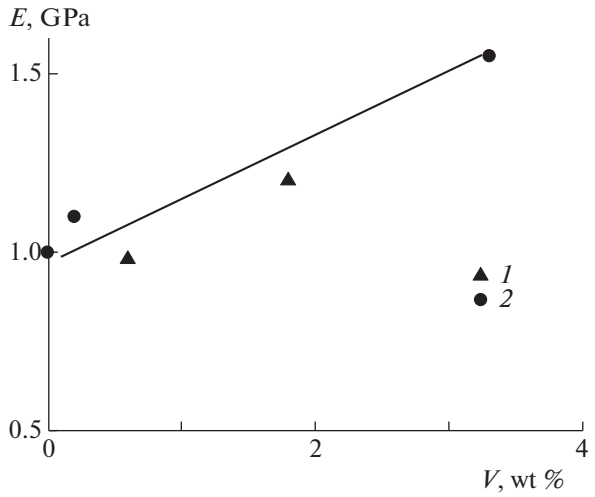

Fig. 8. Dependence of the Young modulus E of unrolled PP on the concentration of the particles of graphene: (*1*) TRG and (*2*) CRG.

the equator and compressed along the meridian. The strain ratio increases with the growth in the degree of cold rolling as a result of the orientation of the plates along the axis of cold rolling.

Figure 10 demonstrates the influence of cold rolling on the stress–strain curves of PP containing V = 0.2 and 3.3 wt % particles. The unrolled composite fractured during the formation of the neck at a strain of ~15% at V = 0.2 wt % (curve *1*). Preliminary cold rolling increased the fracture strain to 400–700%. The neck already stably propagated along the working part of the sample at low degrees of cold rolling (Λ = 1.25), and the fracture occurred at the stage of strain strengthening. In the case of an increase in the degree of cold rolling to Λ = 1.7, the flow of the material became uniform. A growth in the yield point and strength of the material, as well as a certain decrease in the elongation at break, was observed with the increase in Λ, which is explained by the decrease in the deformability of the matrix after cold rolling.

The influence of cold rolling on the behavior of the composite at a degree of filling V = 3.3 wt % is the same (Fig. 10b). The initial composite was brittle, but it underwent fracture during the propagation of the neck after cold rolling of Λ = 1.25-fold. The increase in the degree of cold rolling Λ to 1.7 led to a growth in the elongation at break to 280% and disappearance of the neck. A similar transition from brittle to plastic behavior as a result of cold rolling is also seen in the composites filled with the chemically reduced particles.

The dependence of the Young modulus E of the composite and unfilled PP on the degree of cold rolling Λ is shown in Fig. 11. Cold rolling has almost no influence on the modulus of the matrix and low-filled composite (V = 0.2 wt %). The modulus somewhat decreases at the concentration of particles of 3.3 wt %, apparently, owing to the exfoliation of the particles during rolling because of the nonideal adhesion. Note that the degree of cold rolling was low, and no growth in the Young modulus of PP as a result of molecular orientation was observed.

Microscopy

Figure 12a demonstrates an unrolled sample of PP–0.2% TRG stretched almost to fracture under a transmission electron microscope. It is seen that a rhomboidal microcrack or pore (denoted by the arrow) is present in the formed neck. Oval pores orientated along the axis of drawing are also observed in the neck under higher magnification (Fig. 12b). The micropores are formed by the exfoliation of the particles or fracture of loose agglomerates of particles upon stretching. Rhomboidal pores are also traced in the neck in the case of stretching of the composite containing chemically reduced particles (Fig. 13).

Figure 14 presents the lateral side of the low-temperature chipping of the unrolled composite that underwent fracture upon tension. The SEM image

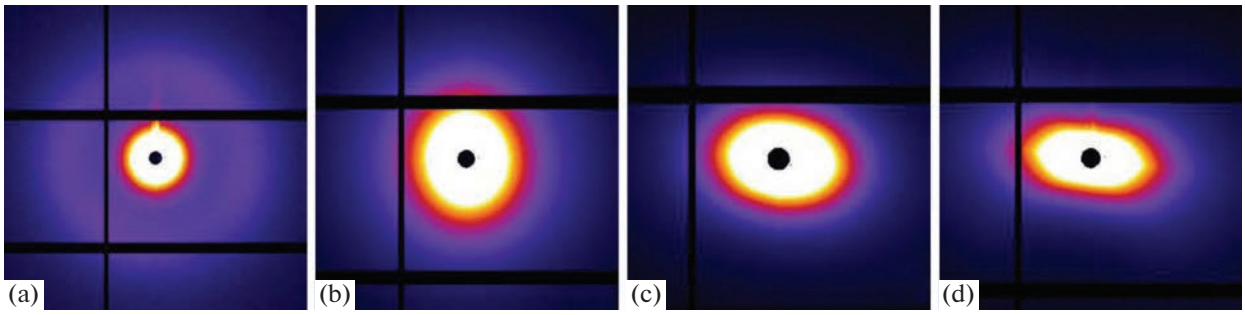

Fig. 9. Small-angle X-ray diffraction patterns of the composites based on PP: (a) initial unrolled PP, (b) unrolled PP–3.3% TRG, (c, d) PP–3.3% TRG with the degree of cold rolling Λ = (c) 1.5 and (d) 2.1. The direction of cold rolling is vertical and the direction of X-rays is parallel to the plane of the film and perpendicular to the direction of cold rolling.

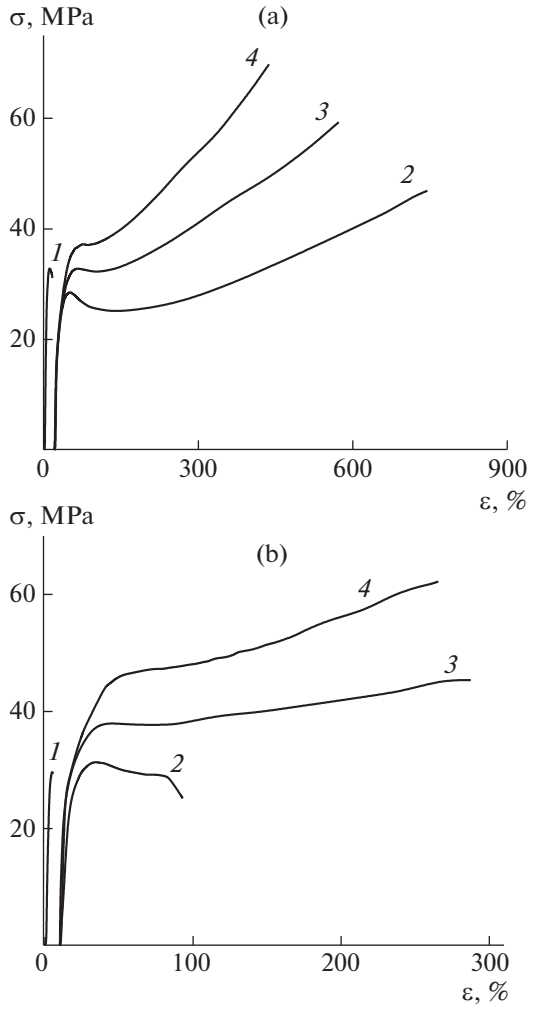

Fig. 10. Stress–strain curves of (*1*) unrolled PP and (*2–4*) rolled PP containing (a) 0.2 and (b) 3.3% TRG; the degree of cold rolling Λ = (*2*) 1.25, (*3*) 1.7, and (*4*) 2.0.

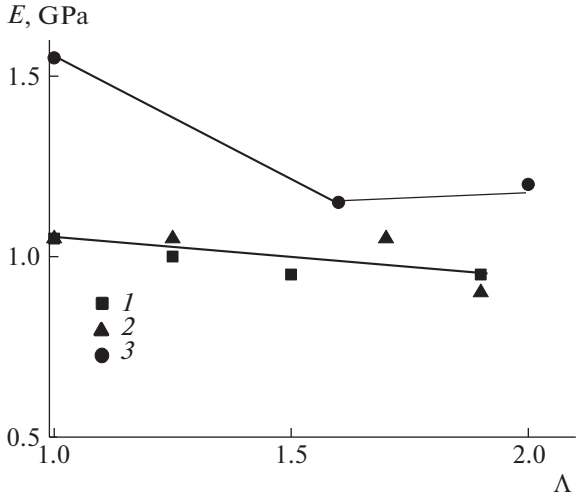

Fig. 11. Dependence of the Young modulus of PP–TRG composites on the degree of cold rolling Λ. The concentration of the particles is (*1*) 0, (*2*) 0.2, and (*3*) 3.3 wt %.

was obtained near the fracture area. The arrow shows a rhomboidal microcrack, in the center of which an agglomerate of particles with a size of ~8 μm and pores elongated along the axis of stretching are seen. The agglomerates initiated the formation of several rhomboidal pores in the neck being formed, one of which led to fracture. As opposed to Figs. 12 and 13, where the rhomboidal pore grows "across the width" of the sample, it increases "through the thickness" in Fig. 14. Having assumed the retention of the volume, the local deformation of the material in the neck was estimated as ~360% from the thickness of the sample in Fig. 14. Note that both uneven areas and microareas of a smooth chipping are observed in this figure. This gives evidence of the presence of the adhesion bonding of the particles with the polymer, as a result of which the particles are not pulled out from the plane of fracture.

Additional information on the fracture of the composites was obtained when using films with a smaller thickness. Figure 15 presents the image of the surface of an unoriented sample with a thickness of 80 μm after fracture under a transmission optical microscope. Upon stretching, the black agglomerates of the particles initiate the appearance of dark stripes (denoted by the arrow) oriented perpendicularly to the axis of stretching. Rhomboidal microcracks are also seen. This makes it possible to draw a conclusion that the agglomerates of the particles initiate the appearance of deformation zones which broaden upon stretching and in which microcracks appear. The transparency of the deformation zones gives evidence of the fact that they are a continuous material rather than crazes. Small oval pores (denoted by the arrow) orientated along the axis of stretching are also observed in the flow zone.

As opposed to the unoriented material, no rhomboidal cracks are formed in the rolled composite. Figure 16 shows a rolled film of the PP–0.2% TRG composite before and after stretching. The aggregates of the particles with a size of 10–50 μm are deformed upon stretching and become elongated together with the polymer matrix along the direction of stretching. Here, neither oval nor rhomboidal pores are formed at a strain of 160%. The size and elongation of the particles indicate that nanoparticles with a size of ~100 nm (see Fig. 1) are assembled into loose optically opaque aggregates with a size of 10–50 μm. Individual nanoparticles are transparent under an optical microscope. The microscopic data also demonstrate that the agglomerates of particles become elongated along the axis of cold rolling during rolling, and their lateral dimensions decrease slightly.

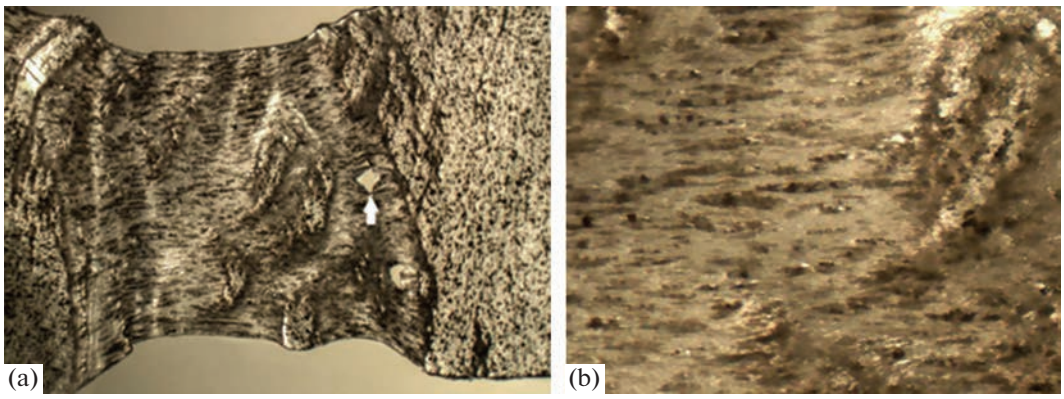

Fig. 12. Optical images of the unrolled sample of PP–0.2% TRG at magnification of (a) ×16 and (b) ×40.

CONCLUSIONS

Nanocomposites have been obtained by in situ filling, i.e., by the synthesis of the PP matrix on graphene-like particles, thus allowing a more uniform distribution of the filler throughout the bulk of the matrix when compared to the mechanical mixing of the particles and the melt of the polymer. Nevertheless, a certain fraction of the particles assembled into agglomerates, while the remaining plates were distributed in the polymer matrix. The agglomerates led to the embrittlement of unrolled PP already at a degree of filling of ~0.2 wt %.

Nanoplates were not pulled out from PP in the case of low-temperature chipping, which indicates the presence of adhesion bonding. The particles increase the Young modulus of the material. Cold rolling leads to a certain decrease in the modulus, apparently, owing to the partial exfoliation of the particles.

Cold rolling suppresses the brittle behavior of the composite irrespective of the method of reduction of the particles of graphite oxide (thermal expansion or chemical).

The agglomerates initiate the appearance of local fluidity microzones, in which the strain of the polymer is high and where microcracks leading to the fracture of the composite are conceived.

Cold rolling up to $\Lambda = 1.25$ suppresses the formation of microzones, and no neck appears at $\Lambda = 1.9$. Pore formation also disappears after cold rolling, and the material does not become turbid in the process of further stretching.

The degree of elongation at break λ is determined from expression (1) in the case of the presence of large defects:

$$\lambda = 1 + \frac{G_{Ic}}{D\sigma}, \qquad (2)$$

where D is the diameter of the agglomerates and σ is the tensile stress.

Figure 17 schematically illustrates the influence of the size of the agglomerates of the particles D on the value of λ. A similar scheme was used by A.F. Ioffe in [44] for the explanation of the change of the mechanism of fracture. Thus, in this figure, curve *1* has been calculated by formula (2), and the degree of elongation at break λ in it is inversely proportional to the size D. Straight line *2* describes the natural elongation at break of the composite λ_m. The fracture occurs upon reaching the minimum of the two values of the elongation at break. In the case of small particles with the size $D < D^*$, the material undergoes fracture at the natural elongation at break of the composite λ_m, and the stress concentration in the agglomerates can be neglected. A change in the mechanism of fracture occurs at $D = D^*$, and the fracture is determined by large agglomerates.

The influence of cold rolling on the mechanism of fracture of the composite is shown in Fig. 18. The dependence of the strain ratio in the neck on the degree of cold rolling Λ is given by curve *1*. The local strain ratio at break (curve *2*) is inversely proportional to the degree of cold rolling Λ [25, 43]: $\lambda = \lambda_0/\Lambda$. Thus, two types of behavior of the composite are possible with the growth in Λ.

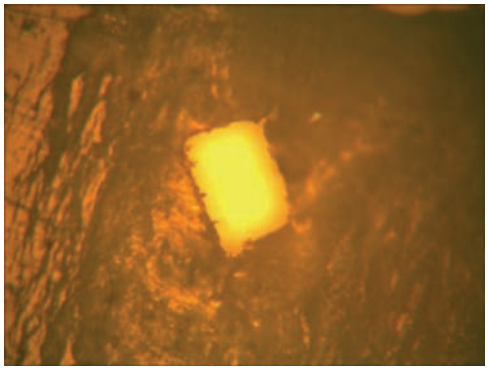

Fig. 13. Optical transmission image of a sample of PP–1.8% CRG at magnification of ×55.

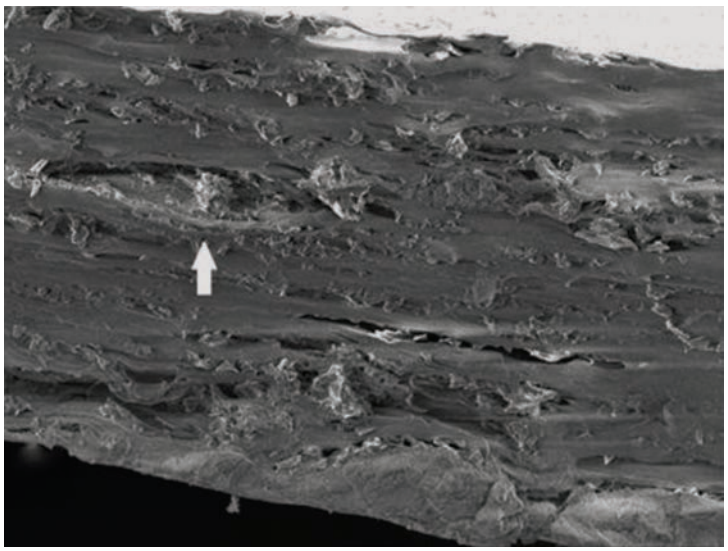

Fig. 14. SEM micrograph of the lateral surface of the chipping of an unrolled sample of PP–1.8% CRG which underwent fracture under stretching; ×1300.

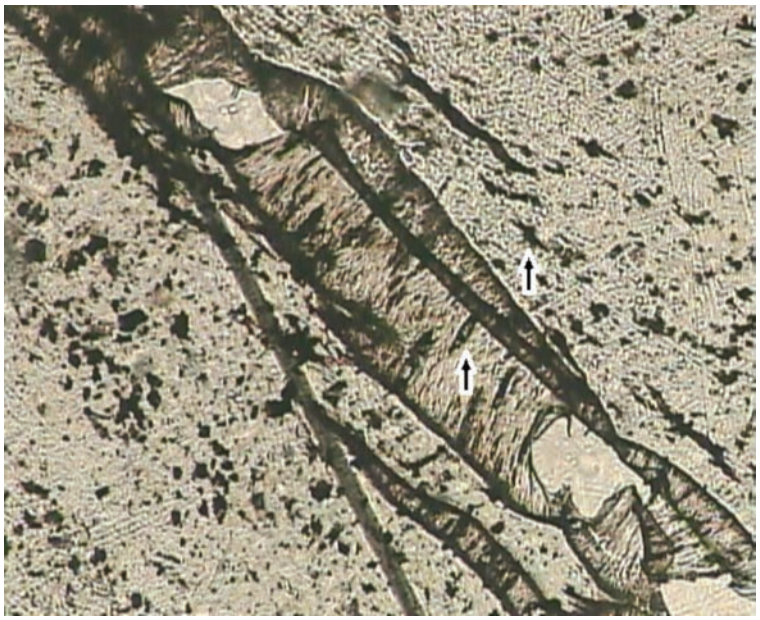

Fig. 15. Optical photographic image of an unrolled sample of PP–0.2% TRG; the thickness of the film is 80 μm; ×80.

The first type—the strain ratio in the case of fracture of the unrolled material is higher than the strain ratio in the neck (curve *2* is higher than curve *1*), and the composite is plastic at all the degrees of cold rolling Λ.

The second type—the strain ratio in the case of fracture of the unrolled material is lower than the strain ratio in the neck (curve *2*'), curve *1* has a greater negative inclination than curve *2*', and there is an intersection of curves *1* and *2*' at a degree of cold rolling Λ*. This corresponds to the change in the mechanism of deformation. At $\Lambda < \Lambda^*$, the elongation ratio at break is lower than the elongation ratio in the neck, and the composite undergoes fracture upon its formation. The neck stably propagates and the composite is plastic at $\Lambda > \Lambda^*$. The transition from brittle to plastic deformation of the composite occurs at $\Lambda = \Lambda^*$. Brittle behavior is observed in the region to the left of the vertical dashed line.

Note that the first type of behavior is generally characteristic of unfilled polymers and composites containing a relatively small amount of small particles.

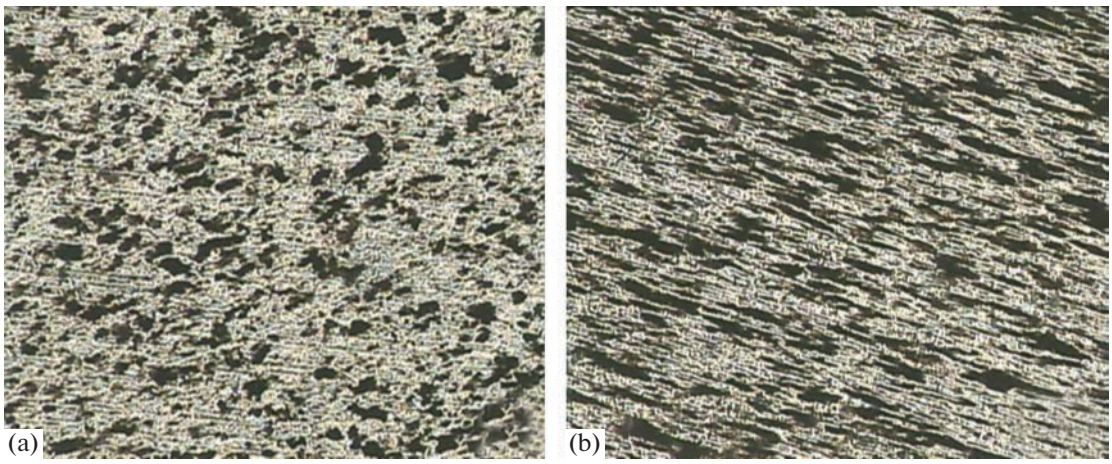

Fig. 16. Micrographs of an unrolled sample of PP–0.2% TRG (the degree of cold rolling $\Lambda = 1.9$) (a) before and (b) after elongation by 160%; ×80.

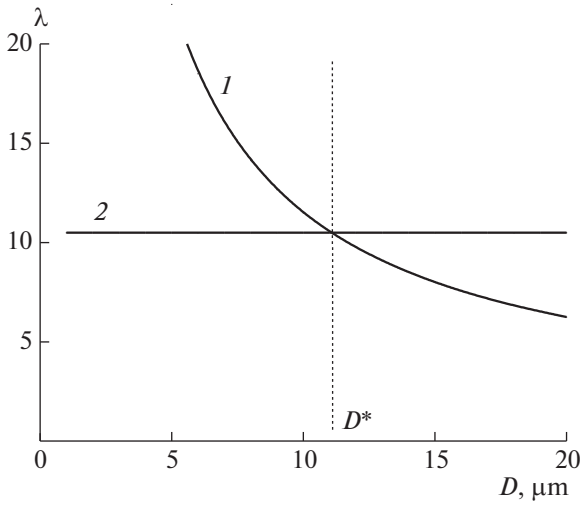

Fig. 17. Influence of the particle size D on the elongation at break of the composite. The explanations are in the text.

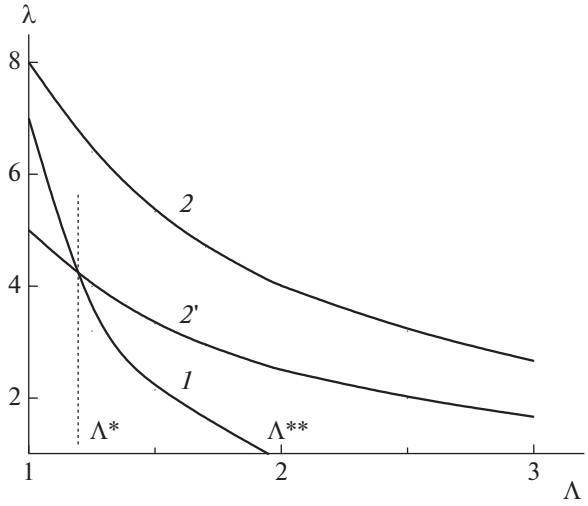

Fig. 18. Influence of the degree of cold rolling Λ (1) on the elongation in the neck and (2, $2'$) in the case of fracture of the composite.

The second type is observed in the case of the use of the composites containing large particles as well as composites with a quite high concentration of small particles.

An increase in the concentration of the particles leads to the shift of curve *2*' downward, and the transition to brittle behavior occurs at a higher degree of cold rolling. The neck disappears at a degree of cold rolling $\Lambda^{**} \sim 2$, and the composite is plastic irrespective of the concentration of the particles.

FUNDING

This work was performed as part of state task no. 0082-2014-0014 and was financially supported by the Russian Foundation of Basic Research (project code 18-33-00573 mol a).

REFERENCES

1. B. C. Brodie, Philos. Trans. R. Soc. London **149**, 249 (1895).
2. W. S. Hummers, Jr. and R. E. Offeman, J. Am. Chem. Soc. **80**, 1339 (1958).
3. A. A. Arbuzov, V. E. Muradyan, and B. P. Tarasov, Russ. Chem. Bull. **62**, 1962 (2013).
4. Y. Qiu, F. Gua, R. Hurt, and I. Kulaots, Carbon **72**, 215 (2014).
5. T. M. Ushakova, E. E. Starchak, V. G. Krasheninnikov, V. G. Grinev, T. A. Ladygina, and L. A. Novokshonova, J. Appl. Polym. Sci. **131**, 40151 (2014).

6. A. L. Margolin, T. V. Monakhova, P. M. Nedorezova, A. N. Klyamkina, and S. V. Polschikov, Polym. Degrad. Stab. **156**, 59 (2018).

7. F. S. D'yachkovskii and L. A. Novokshonova, Russ. Chem. Rev. **53**, 117 (1984).

8. L. A. Novokshonova and I. N. Meshkova, Vysokomol. Soedin., Ser. A **36**, 629 (1994).

9. V. A. Tochin, E. N. Shchupak, V. V. Tumanov, O. B. Kulachinskaya, and M. I. Gai, Mekhan. Kompoz. Mater., No. 4, 635 (1984).

10. V. A. Topolkaraev, N. V. Gorbunova, I. L. Dubnikova, T. V. Paramzina, and F. S. D'yachkovskii, Vysokomol. Soedin., Ser. A **32**, 2210 (1990).

11. S. L. Bazhenov, J. X. Li, A. Hiltner, and E. Baer, J. Appl. Polym. Sci. **52**, 243 (1994).

12. S. L. Bazhenov, in *Plastics Additives,* Ed. by G. Pritchard (Chapman and Hall, London, 1998).

13. S. L. Bazhenov, A. A. Berlin, A. A. Kul'kov, and V. G. Oshmyan, *Polymer Composite Materials. Strength and Technology* (Intellekt, Moscow, 2010) [in Russian].

14. S. L. Bazhenov, O. A. Serenko, I. L. Dubnikova, and A. A. Berlin, Dokl. Phys. **48**, 640 (2003).

15. O. A. Serenko, S. L. Bazhenov, I. N. Nasrullaev, and Al. Al. Berlin, Polym. Sci., Ser. A **47**, 49 (2005).

16. L. Nielsen, *Mechanical Properties of Polymers and Composites* (Marcel Dekker, New York, 1974).

17. S. L. Bazhenov, V. G. Grinev, O. I. Kudinova, and L. A. Novokshonova, Polym. Sci., Ser. A **52**, 549 (2010).

18. I. L. Dubnikova, V. A. Topolkaraev, T. V. Paramzina, E. V. Gorokhova, and F. S. D'yachkovskii, Vysokomol. Soedin., Ser. A **32**, 841 (1990).

19. O. A. Serenko, V. S. Avinkin, and S. L. Bazhenov, Polym. Sci., Ser. A **44**, 286 (2002).

20. O. A. Serenko, E. S. Obolonkova, S. L. Bazhenov, A. V. Efimov, A. L. Volynskii, and I. N. Nasrullaev, Polym. Sci., Ser. A **45**, 773 (2003).

21. Y. Hernandez, T. Lozano, A. B. Morales, F. N. Pardo, P. G. Lafleur, S. Sanchez-Valdes, G. Martinez-Colunga, L. Morales-Zamudio, and P. De Lira-Gomez, J. Compos. Mater. **51**, 373 (2017).

22. B. San, H. B. Waisman, and H. Waisman, J. Appl. Mech., Trans. ASME **842** (2), 021005 (2017).

23. N. Sandeep, S. P. Tripathi, and G. S. S. Rao, RSC Adv. **7**, 23615 (2017).

24. I. V. Tyunkin, S. L. Bazhenov, A. S. Kechekyan, A. V. Efimov, and S. A. Timan, Polym. Sci., Ser. A **53**, 715 (2011).

25. S. L. Bazhenov, A. V. Bobrov, A. V. Efimov, T. E. Grokhovskaya, and A. S. Kechekyan, Polym. Sci., Ser. A **57**, 285 (2015).

26. D. M. Gezovich and P. H. Geil, J. Mater. Sci. **6**, 531 (1971).

27. V. A. Marikhin, L. P. Myasnikova, I. I. Novak, V. A. Suchkov, and M. Sh. Tukhvatulina, Vysokomol. Soedin., Ser. A **14**, 2457 (1972).

28. K. Nakayama, K. Qi, and X. Hu, Polym. Compos. **9**, 151 (2001).

29. D. Raabe, N. Chen, and L. Chen, Polymer **45**, 8265 (2004).

30. J. Jia, D. Raabe, and W. M. Mao, Chin. J. Polym. Sci. **24**, 403 (2006).

31. K. Kosugi, T. Yokoyama, and T. Yamada, Jpn. Soc. Exp. Mech. **8** 71 (2008).

32. J. Qiu, M. Kawagoe, W. Mizuno, and M. Morita, Trans. Jpn. Soc. Mech. Eng. A **66**, 867 (2000).

33. Y. J. Phua, W. S. Chow, and Z. A. Mohd Ishak, eXPRESS Polym. Lett. **5**, 93 (2011).

34. J. Qiu, T. Murata, K. Takahashi, and X. Wu, Adv. Mater. Res. **391–392**, 585 (2012).

35. P. A. Kechek'yan, A. S. Kechek'yan, and S. L. Bazhenov, Polym. Sci., Ser. A **60**, 373 (2018).

36. K. Z. Monakhova, S. L. Bazhenov, and A. S. Kechek'yan, Polym. Sci., Ser. A **61**, 499 (2019).

37. P. M. Nedorezova, V. I. Tsvetkova, A. M. Aladyshev, D. V. Savinov, A. N. Klyamkina, V. A. Optov, and D. A. Lemenovskii, Polym. Sci., Ser. A **43**, 356 (2001).

38. V. E. Muradyan, V. S. Romanova, A. P. Moravsky, Z. N. Parnes, and Yu. N. Novikov, Russ. Chem. Bull. **49**, 1017 (2000).

39. A. A. Arbuzov, V. E. Muradyan, and B. P. Tarasov, Izv. Akad. Nauk, Ser. Khim., No. 9, 1962 (2013).

40. S. V. Polschikov, P. M. Nedorezova, A. N. Klyamkina, A. A. Kovalchuk, A. M. Aladyshev, A. N. Shchegolikhin, V. G. Shevchenko, and V. E. Muradyan, J. Appl. Polym. Sci. **127**, 904 (2013).

41. P. M. Nedorezova, V. G. Shevchenko, A. N. Shchegolikhin, V. I. Tsvetkova, and Yu. M. Korolev, Polym. Sci., Ser. A **46**, 242 (2004).

42. D. I. Svergun and L. A. Feigin, *Small-Angle X-ray and Neutron Scattering* (Nauka, Moscow, 1986) [in Russian].

43. I. V. Tyun'kin, Candidate's Dissertation in Chemistry (Inst. Khim. Fiz. RAN, Moscow, 2011).

44. A. F. Ioffe, M. V. Kirpicheva, and M. A. Levitskaya, Zh. Russ. Fiz.-Khim. Obshch. **56**, 489 (1924).

Translated by E. Boltukhina

SPELL: 1. embrittlement, 2. embrittled